Northumbria
University
NEWCASTLE

Novel Bearingless Switched Reluctance Motor with Wide Flat Inductance Region to Simplify the Control of Torque and Levitation Force

Zhenyang Hao, Xin Cao, *Member, IEEE*, Xu Deng, Xiang Shen

***Abstract*—In conventional 12/8 bearingless switched reluctance motors (BSRMs), the generation and control of torque and levitation forces are always coupled and interacted, which increases the complexity of the current control algorithm. In this paper, a novel BSRM with 12 stator poles and 4 rotor poles is proposed to simplify the control of torque and levitation, which has wide flat inductance region. Through allocating the generation of torque and levitation forces to different inductance regions of each phase, the levitation control can be similar as that of magnetic bearings, and the torque control can adopt the methods of conventional switched reluctance motors, e.g. current chopping control and angle position control. Accordingly, the current control algorithm of proposed BSRM becomes very easy and flexible. Extensive experiments were completed to verify the demonstrated performance of proposed motor.**

***Index Terms*—Bearingless switched reluctance motor, torque, levitation force, current chopping control, angle position control.**

NOMENCLATURE

α, β	Displacements on the direction of α-axis and β-axis, respectively
$\bar{i_a}$	Average current of phase A
Δi_{a1}, Δi_{a2}	Differences of phase-A winding currents on the direction of α-axis and β-axis, respectively
Φ_{a1}-Φ_{a4}	Main flux of four phase-A windings, respectively
Φ_{b1}-Φ_{b4}	Main flux of four phase-B windings, respectively
μ_0	Permeability of vacuum
θ	Rotor angle position
a	Constant 1.01
F_α, F_β	Radial forces on the direction of α-axis and β-axis, respectively
h	Lamination length of the iron core
i_α^*, i_β^*	Required levitation currents on the direction of α-axis and β-axis, respectively
i_T^*	Required torque current
i_{a1}-i_{a4}, i_{b1}-i_{b4}	Winding currents of phases A and B, respectively
l_0	Air-gap length between the stator and rotor poles
N_s	Number of winding turns
P_{a1}-P_{a4}	Air-gap permeances of phase A, respectively
P_{b1}-P_{b4}	Air-gap permeances of phase B, respectively
r	Radius of rotor
U_{dc}	Direct voltage for excitation

Manuscript received . This work was supported by the National Natural Science Foundation of China, under Grant No. 51877107. *(Corresponding author: Xin Cao.)*

Zhenyang Hao and Xin Cao are with Department of Electrical Engineering and also with the Center for More-Electric-Aircraft Power System, Nanjing University of Aeronautics and Astronautics, Nanjing, 211106, China (e-mail: zhenyang_hao@nuaa.edu.cn; caoxin@nuaa.edu.cn).

Xu Deng is with School of Engineering, Newcastle University, Newcastle upon Tyne NE1 7RU, U.K. (e-mail: xu.deng@ncl.ac.uk).

Xiang Shen is with Department of Mechanical and Construction Engineering, Northumbria University, Newcastle upon Tyne NE1 8ST, U.K. (e-mail: x.shen@outlook.com).

I. INTRODUCTION

SWITCHED Reluctance Motor (SRM) consists of a salient-pole stator installed with concentrated windings and a salient-pole rotor without any windings and permanent magnets, thus it has the advantages of simple structure, easy control, high-speed ability and strong fault-tolerant capability [1]–[4]. Combining the function of magnetic bearing with SRMs, the bearingless switched reluctance motor (BSRM) has been proposed to achieve the magnetic levitation when the rotor is rotating at a high speed [5]. In addition to having advantages of conventional SRMs, BSRMs can avoid the friction and lubrication caused by the mechanical bearing. Therefore, the research on BSRMs has been developed greatly in past decades.

The first prototype of BSRMs was implemented by M. Takemoto et. al. [6], which has two sets of windings installed in the stator. The rotation control and levitation control are implemented by the two sets of windings, respectively. Due to the coupling between the two windings, the mathematical models of torque and levitation forces were established and several control methods were also proposed [7]–[9]. In addition, some BSRMs with only one set of windings were also proposed and developed to achieve the rotation and levitation simultaneously [10]–[15]. However, the control algorithm is always very complex because the generations of torque and levitation forces are strongly coupled [8], [12], [14]. Therefore, two kinds of approaches were developed to achieve the simultaneous control between torque and levitation forces. One is to design particular control algorithm for conventional structures of BSRMs, e.g. independent control, direct torque and levitation-force control, and some intelligent control methods [16]–[20]. The other approach is to develop novel structures for the decoupling control of torque and levitation forces. This concept was firstly employed to propose the 8/10 BSRM [21], [22], which allocates the rotation and levitation control to different stator-pole windings. Accordingly, the torque control is independent from the levitation-force control which makes the drive system simple and easy. However, the flux paths for the generation of torque and levitation forces have partial crossing [22]. In addition, the 8/10 BSRM is a single-phase motor, thus it could generate large torque ripple [23]. Therefore, the two-phase 12/14 BSRM was proposed to further reduce the coupling between the torque and levitation forces

[23], [24]. Moreover, a 12/8 BSRM with two stators and one rotor was studied to reduce the torque ripple in addition to the decoupling control of the torque and levitation forces. The outer stator windings are excited to provide the torque whereas the inner stator windings to provide levitation forces. Accordingly, the generations of torque and levitation forces are decoupled from the operation principle.

In summary, the aforementioned structures to decouple the control of torque and levitation forces usually divide all stator poles into two parts: one is to generate torque and the other is to generate levitation forces. In this paper, we attempt to allocate the torque and levitation-force control into different inductance regions of each phase, and then the rotation and levitation can be achieved simultaneously. Therefore, the 12/4 BSRM is investigated and implemented to obtain a high-speed BSRM with advantages of simple structure and easy control. The torque and levitation forces are regulated in different inductance regions of each phase respectively, i.e. the torque and levitation can be controlled independently..

The rest of this paper is organized as follows. In Section II, the principle of proposed 12/4 BSRM is demonstrated in detail and the derivation of the mathematical model is introduced briefly. Accordingly, the levitation-force control and torque control are illustrated by designing the winding current algorithm and control block in Section III. Experimental results are provided in Section IV, and conclusion is made in Section V.

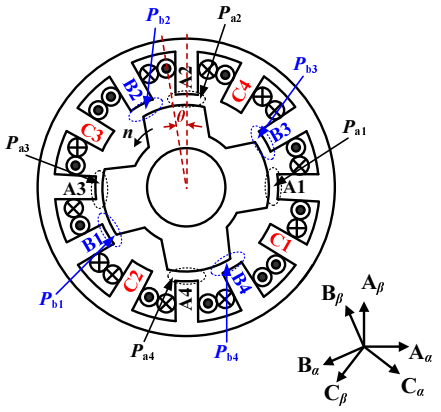

Fig. 1. Structure of proposed 12/4 BSRM.

II. Principle of Proposed 12/4 Bearingless Switched Reluctance Motor

A. Generations of Torque and Levitation Force

In the proposed 12/4 BSRM, twelve coils are mounted on the twelve stator poles and each phase winding consists of four coils, as shown in Fig. 1, where θ is the intersection angle between the two axes of the stator and rotor poles. The coil current on each stator pole is regulated independently, thus the radial force acted on the rotor can be produced by conducting different currents in the four coils of each phase. In order to produce the positive torque, the coil current only conducts in the inductance-ascending region.

Fig. 2 shows the coil-inductance curves of three phases, where $\theta = 0^\circ$ represents that the stator and rotor poles of phase A are aligned straightly. Due to the 12/4 structure, the width of the flat region for the maximum inductance is 30°. For the production of electromagnetic torque, this kind of wide flat region should not be appeared in conventional SRMs. However, this flat region of the maximum inductances can be used to produce levitation forces in BSRMs, which can provide large radial forces more efficiently. More importantly, the control of levitation forces can be similar as that in magnetic bearings, which means the levitation control can be easier than that in conventional 12/8 BSRMs. In addition, these flat regions in three phases appear alternately and are continuous in one electrical period. Therefore, the radial forces of three phases can be provided continuously in the flat region for the levitation.

Fig. 2 shows the generations of torque and radial forces by each phase in different inductance regions. The torque is produced in the inductance-ascending region and the levitation forces are produced in the flat region of the maximum inductance. Taking phase A as the example, when $\theta \in [-45^\circ, -15^\circ]$, the four coils are conducted with the same current to generate positive torque. When $\theta \in [-15^\circ, 15^\circ]$, the four coils are conducted with different currents to generate levitation forces. Therefore, the torque and levitation forces can be generated in different inductance regions of one phase, thus they can be regulated by different control variables. The torque control is more flexible than that in conventional 12/8 BSRMs. The current chopping control (CCC), angle position control (APC) and PWM control which are generally used in SRM control, can be applied in the torque control of the proposed BSRM. In addition, since the levitation forces are generated in the constant inductance region, the levitation can be implemented similarly as that in magnetic bearings.

In order to analyze the generation of torque and levitation forces, the flux-line distribution has been investigated at different rotor angle positions with Ansoft Maxwell simulation, as shown in Fig. 3. Where, $i_{aa1} = i_{a2} = 2$A, $i_{a3} = i_{a4} = 1$A, and $i_{b1} = i_{b2} = i_{b3} = i_{b4} = 2$A. From Figs. 2 and 3, the torque is generally produced in the inductance-ascending region of phase B, and the levitation forces can be effectively generated by phase A which is located in the maximum inductance region. However, there are almost no flux-line passing through stator poles of phase B when they do not overlap with rotor poles. Therefore, the output torque of proposed 12/4 BSRM cannot be provided continuously. In order to overcome this defect, two 12/4 BSRMs can be installed in parallel. The stator poles of two BSRMs are lined up exactly, and the rotor poles are assembled on the shaft with 15° shifted as shown in Fig. 4. It can be seen that the inductance-ascending regions of two motors are continuous, hence the output torque on the same shaft can be generated continuously. Moreover, the shaft can be levitated with four degree-of-freedoms (DOFs) by the two BSRMs. In this paper, it is focused on the principle and implementation of the proposed 12/4 BSRM, thus the study on the two parallel BSRMs is not included.

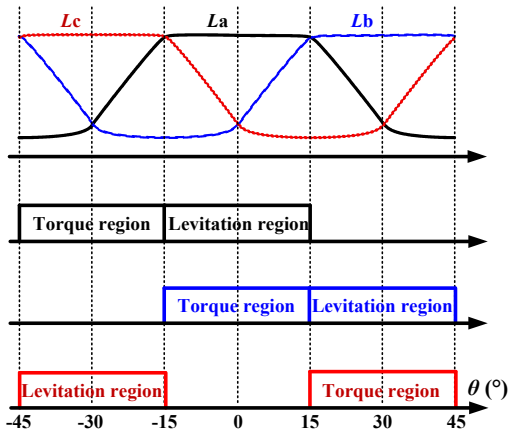

Fig. 2. Inductance curves of three phases.

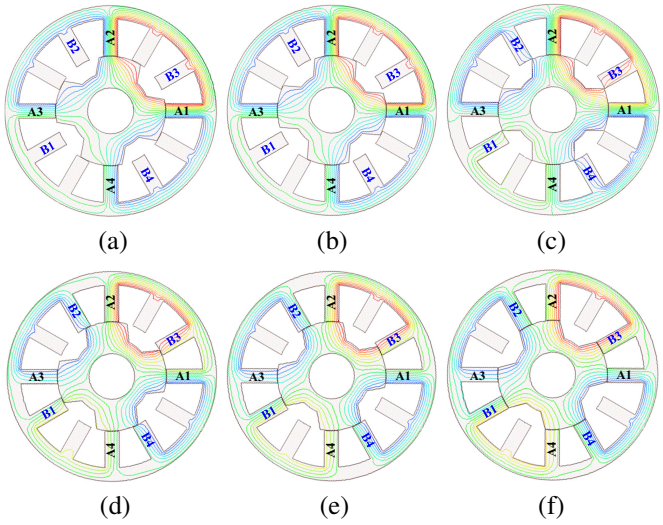

Fig. 3. Flux-line distribution with Ansoft Maxwell simulation at different rotor angle positions: (a)$\theta = -10°$. (b) $\theta = -5°$. (c) $\theta = 0°$. (d) $\theta = 5°$. (e) $\theta = 10°$. (f) $\theta = 15°$.

B. Finite Element Analysis (FEA) of Proposed BSRM

In order to investigate the relationship between the torque and levitation forces, FEA was completed using the software of Ansoft Maxwell with motor parameters listed in Table I.

TABLE I
PARAMETERS OF STUDIED BSRM

Parameters	Values
Number of winding turns	42 turns
Arc angle of stator poles	15 degree
Arc angle of rotor poles	45 degree
Outside diameter of stator core	115 mm
Inside diameter of stator pole	60.2 mm
Radius of rotor pole, r	29.85 mm
Stack length lamination, h	48 mm
Average air-gap length between rotor and stator, l_0	0.25 mm
Average air-gap length between shaft and backup bearing	0.2 mm

Fig. 5 shows FEA results to demonstrate the relationship between the generations of torque and levitation force with different winding currents, where the winding currents in different cases are listed in Table II and they have rectangular-

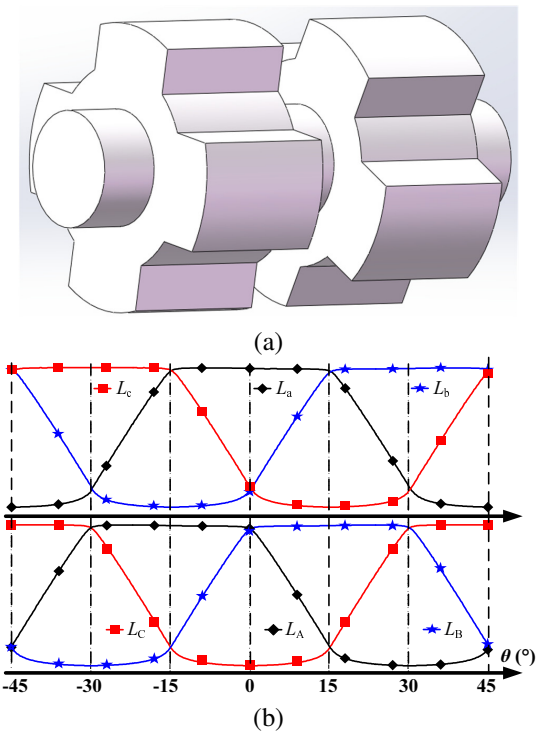

Fig. 4. Structure and inductances of two parallel BSRMs with 15° shifted: (a) Rotor structure. (b) Phase inductances of two motors.

like current waveforms in one electric period. The excitation region is $\theta \in [0, 15°]$, as illustrated in Fig. 2, where phase A locates in the flat region of the maximum inductances whereas phase B locates in its inductance-ascending region. Therefore, phase A is excited to provide the levitation force and phase B is excited to provide the torque. For cases 1, 2, 3 and 4, torque currents i_{b1}, i_{b2}, i_{b3} and i_{b4} are always 2A, whereas levitation currents i_{a1}, i_{a2}, i_{a3} and i_{a4} are changed to illustrate how levitation currents affect the generation of torque. For cases 5, 6, 7 and 8, levitation currents i_{a1}, i_{a2}, i_{a3} and i_{a4} keep the same value, whereas torque currents i_{b1}, i_{b2}, i_{b3} and i_{b4} are changed to illustrate how torque currents affect the generation of levitation forces. In Fig. 5(a), the generated torque is almost the same though by different levitation currents in the region of $\theta \in [0, 12°]$. Due to the increased fringing flux in the region of $\theta \in [12°, 15°]$, the torque becomes different when the levitation current changes. In Fig. 5(b) and (c), F_β keeps the same value approximately in the region of $\theta \in [0, 15°]$, whereas the difference of F_α increases gradually with the increase of θ. When $\theta = 15°$, F_α is reduced by 10.07% with torque currents increased from 0 to 3A. However, the influence of torque current on the levitation force has been greatly reduced compared with conventional 12/8 BSRMs, and this influence can be compensated by the PID controller of levitation control.

C. Comparison between Proposed 12/4 BSRM and Conventional 12/8 BSRM

In order to clarify the characteristics of proposed 12/4 BSRM, the comparison based on FEA method has been

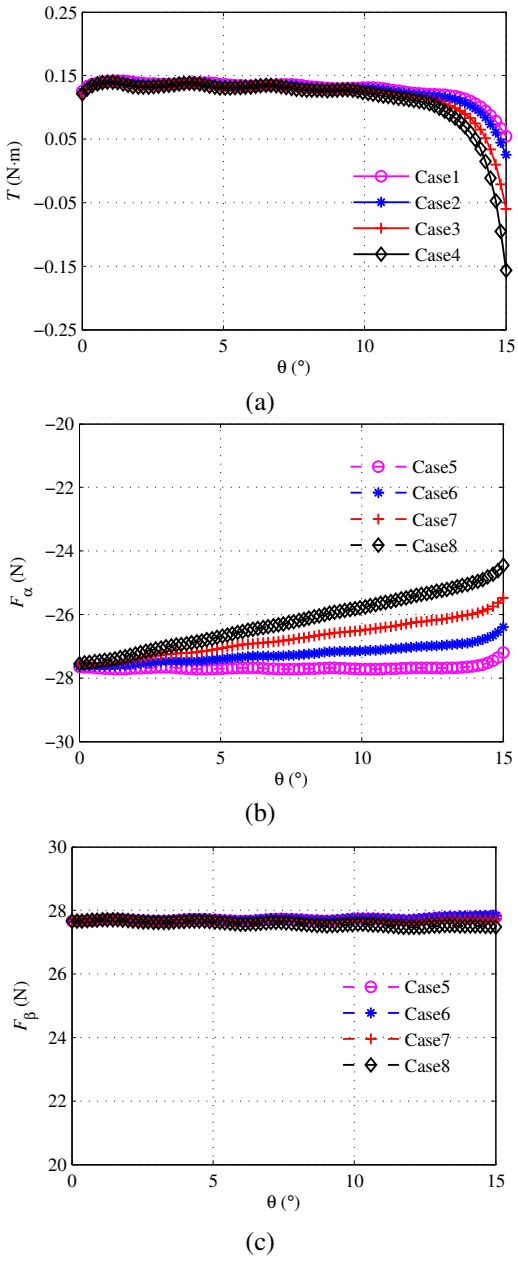

Fig. 5. FEA results of torque and levitation forces with different winding currents: (a) Torque. (b) α-axis levitation force F_α. (c) β-axis levitation force F_β.

completed between proposed 12/4 BSRM and conventional 12/8 BSRM. Most of the parameters of the two motors are the same as listed in Table I, whereas the differences are the rotor-pole number and the arc angle of rotor poles. In the analyzed 12/8 BSRM, the rotor-pole number is 8, and the arc angle of rotor poles is 15°. Only phase-A windings are excited in one electric period with currents listed in Table III.

Figs. 6 and 7 show the generated torque and levitation forces of the two motors in one electric period, respectively. For the two motors, the maximum torque and maximum levitation forces that they can provided are identical approximately. Differently, the levitation forces can be provided with the maximum value within 1/3 electric period in 12/4 BSRM,

Table II
CASES IN FEA WITH DIFFERENT WINDING CURRENTS (A).

Case	i_{a1}	i_{a2}	i_{a3}	i_{a4}	i_{b1}	i_{b2}	i_{b3}	i_{b4}
1	0	0	0	0	2	2	2	2
2	1	2	2	1	2	2	2	2
3	2	4	4	2	2	2	2	2
4	3	6	6	3	2	2	2	2
5	1	2	2	1	0	0	0	0
6	1	2	2	1	1	1	1	1
7	1	2	2	1	2	2	2	2
8	1	2	2	1	3	3	3	3

i.e. $\theta \in [-15^\circ, 15^\circ]$, but no torque can be generated in this region. In other words, the positive torque and negative torque are both sacrificed to obtain maximum and constant levitation forces in the 12/4 BSRM. The benefits are constant and larger levitation forces as well as the simple levitation control. In the 12/8 BSRM, the positive torque and levitation forces are provided in the same region, i.e. $\theta \in [-15^\circ, 0]$. The torque and levitation forces are determined by the same winding currents. Therefore, the torque control and levitation-force control are coupled through winding currents, hence the complex current control algorithm is required.

Table III
PHASE-A WINDING CURRENTS FOR THE COMPARISON BETWEEN 12/4 AND 12/8 BSRMS (A).

Group	i_{a1}	i_{a2}	i_{a3}	i_{a4}
1	1	1	1	1
2	2	2	2	1
3	3	3	3	3
4	1	2	2	1
5	2	4	4	2
6	3	6	6	3

In summary, the proposed BSRM is good at the large levitation-force generation and the simple levitation control. The shortcoming is the discontinuous generation of torque, which is mainly caused by the wide flat inductance region. The flat region of maximum inductance is beneficial to the generation and control of levitation forces, but the inductance-ascending region is narrowed. Therefore, the structure of two parallel installed BSRMs can be used to overcome this defect as illustrated in Fig. 4, which could achieve 4-DOF magnetic levitation.

From the analysis mentioned above, the proposed 12/4 BSRM is well-suited for the applications with large radial-force loads, e.g. the high-power driving system with a heavy rotor. It is also well-suited for the high-speed rotating system with large vibrations, e.g. More-Electric-Aircraft engine system in which it can be used as a starter and generator.

D. Mathematical Model of Torque and Levitation Forces

From the analysis mentioned above, the torque and levitation force can be generated by different control variables. For the torque control, the conventional torque control methods of SRMs can be used in the region of $\theta \in [-45^\circ, -15^\circ]$. For the levitation control, the typical PID controller can be used to obtain the levitation currents. However, to investigate the relationship among the torque, levitation forces, rotor angle

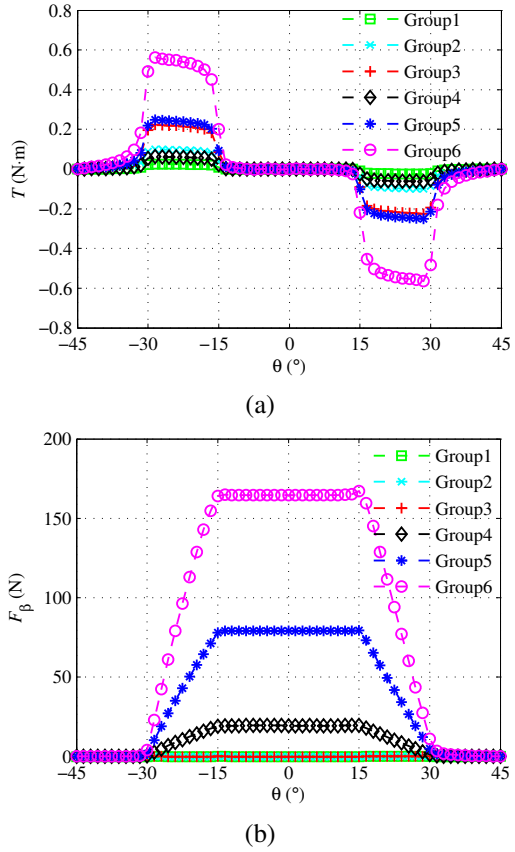

Fig. 6. FEA results of 12/4 BSRM: (a) Torque. (b) Levitation force.

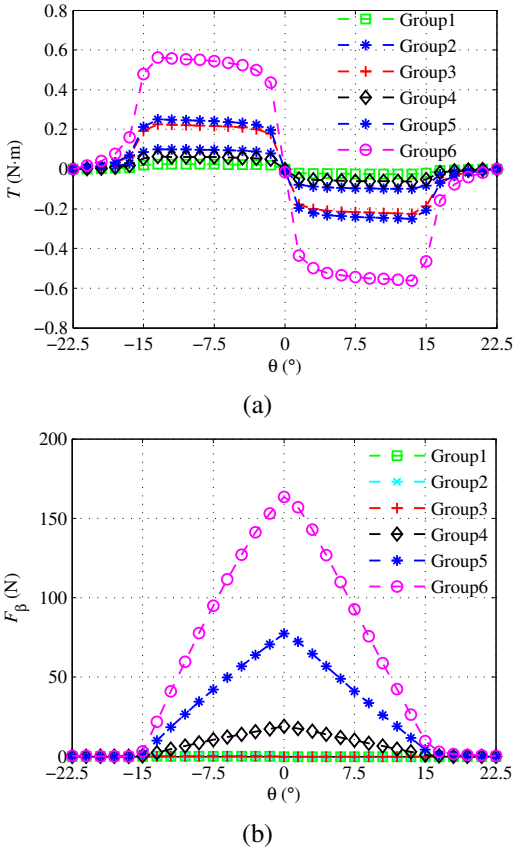

Fig. 7. FEA results of 12/8 BSRM: (a) Torque. (b) Levitation force.

position and the winding currents, the mathematical models of torque and levitation forces should be established, which is also helpful to design the control algorithm of proposed BSRMs.

According to virtual-work method adopted in conventional BSRMs, the air-gap magnetic permeances of excited phase poles should be established firstly [8], [25]. Considering that two phases are excited simultaneously, the rotor angle position and the magnetic permeance can be illustrated in Fig. 8. Based on the conventional magnetic-permeance modelling method, P_{a1} and P_{b3} can be respectively obtained as (1) and (2).

Similarly, P_{a2}-P_{a4}, P_{b1}, P_{b2} and P_{b4} can also be obtained to facilitate the modeling of magnetic flux linkages. The equivalent magnetic circuits considering phases A and B can be illustrated in Fig. 9. Therefore, the inductances of the two phases can be obtained, which are relevant to P_{a1}-P_{a4} and P_{b1}-P_{b4}. Accordingly, the magnetic energy is then calculated by the inductance matrix and phase-winding currents. Finally, the expressions of torque and levitation forces can be derived by calculating the partial derivatives of magnetic energy with respect to rotor angle position and radial displacements α and β.

III. Levitation Force and Torque Control

In conventional BSRMs, the levitation control should be implemented together with the torque control, thus the winding currents are calculated from a designed and always complex

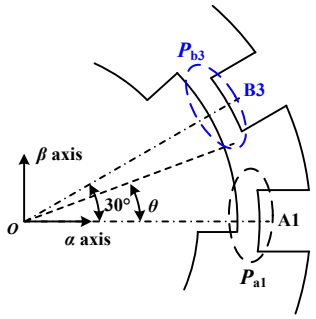

Fig. 8. Schematic view of the air-gap magnetic permeance.

current algorithm. In the proposed BSRM, the levitation-force control is independent from the torque control because of the production of torque and levitation forces in different regions. In the torque region, the torque can be controlled like conventional SRMs. In the levitation-force region, the levitation-current algorithm of four windings can also be designed simply to obtain the required levitation forces.

A. Current Algorithm

Fig. 10 shows the current algorithm of phase A to demonstrate how to regulate the phase-winding currents for the rotation and levitation. In this paper, conventional CCC and APC methods are employed to regulate the torque in the torque region, and the current hysteresis-loop control is employed to

$$P_{a1}=\frac{\mu_0 hr\pi\left(l_0+\alpha\right)}{12l_0^2}+\frac{\mu_0 h}{\pi\left(\pi a-2\right)}\left\{\begin{array}{l}\pi a\ln\left[\frac{12a^2l_0^3+arl_0(l_0-\alpha)(2\pi-12\theta)+\pi r^2(l_0+2\alpha)(\pi/12-\theta)}{12a^2l_0^3}\right]\\+(\pi a-4)\ln\left[\frac{48l_0^3+\pi rl_0(l_0+\alpha)(4\pi-24\theta)+\pi^3r^2(l_0+2\alpha)(\pi/12-\theta)}{4l_0^3}\right]\end{array}\right\},\tag{1}$$

$$P_{b3}=\frac{\mu_0 hr\theta\left(2l_0+\sqrt{3}\alpha+\beta\right)}{2l_0^2}+\frac{\mu_0 h}{\pi\left(\pi a-2\right)}\left\{\begin{array}{l}\pi a\ln\left[\frac{12a^2l_0^3+arl_0\left(2l_0+\sqrt{3}\alpha+\beta\right)(\pi-6\theta)+\pi r^2\left(l_0+\sqrt{3}\alpha+\beta\right)(\pi/12-\theta)}{12a^2l_0^3}\right]\\+(\pi a-4)\ln\left[\frac{48l_0^3+\pi rl_0\left(2l_0+\sqrt{3}\alpha+\beta\right)(2\pi-12\theta)+\pi^3r^2\left(l_0+\sqrt{3}\alpha+\beta\right)(\pi/12-\theta)}{48l_0^3}\right]\end{array}\right\}.\tag{2}$$

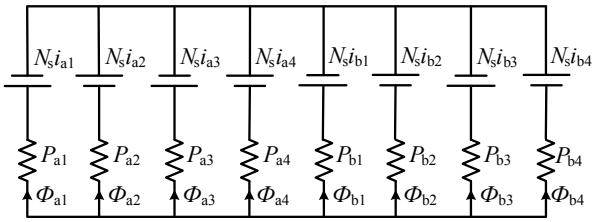

Fig. 9. Equivalent magnetic circuits of proposed BSRM.

regulate the levitation force in the levitation region. It can be seen that levitation forces can be provided by three phases alternately.

In the CCC method, the power switches of one phase are chopped to track the reference value of the phase-winding current, thus the real current has a rectangular waveform in one control period. The output torque can be regulated by changing the reference current. In APC method, the power switches of one phase are switched only one time in each control period, and the turn-ON angle is usually the control target to regulate the current waveform. Therefore, CCC and APC methods can both regulate the output torque by changing the current waveform, as illustrated in Fig. 10.

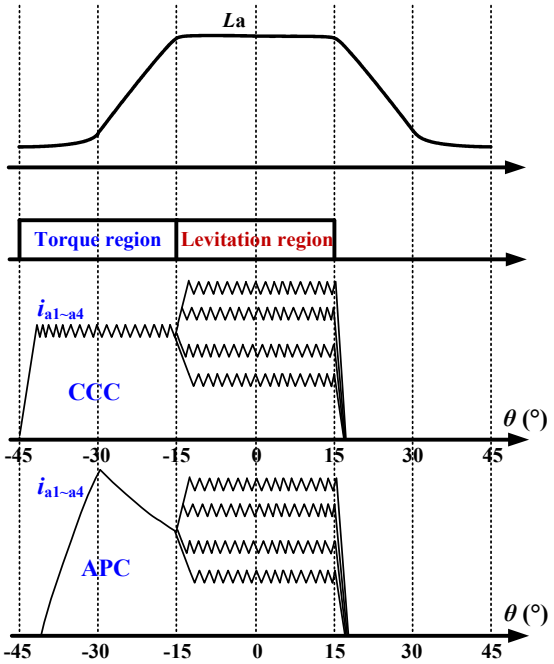

Fig. 10. Schematic diagram of phase-A currents

From demonstrated model in Subsection II-D, the levitation force is relevant to rotor angle position and motor mechanical parameters. To obtain a certain levitation force, the required winding currents should be calculated from the derived models, which means that a complex current calculation process is necessary. In order to simplify the current algorithm, the average phase current $\bar{i}$ is introduced. Taking phase A as an example, its average current $\bar{i_a}$ can be written as

$$\bar{i_a}=\frac{i_{a1}+i_{a3}}{2}=\frac{i_{a2}+i_{a4}}{2}.\tag{3}$$

Accordingly, the differences of winding currents in two directions can be expressed by

$$\Delta i_{a1}=\frac{|\,i_{a1}-i_{a3}\,|}{2},\tag{4}$$

$$\Delta i_{a2}=\frac{|\,i_{a2}-i_{a4}\,|}{2}.\tag{5}$$

Therefore, the expressions of levitation forces can be simplified as

$$F_\alpha=4K_{f1}\left(\theta\right)\bar{i_a}\Delta i_{a1},\tag{6}$$

$$F_\beta=4K_{f1}\left(\theta\right)\bar{i_a}\Delta i_{a2}.\tag{7}$$

Where, the coefficient $K_{f1}\left(\theta\right)$ is the levitation-force coefficient which is relevant to the rotor angle position and mechanical parameters of the motor. Considering that the levitation forces are only produced in the flat inductance region, i.e. $\theta\in[-15°,15°]$ as illustrated in Fig. 2, the coefficient $K_{f1}\left(\theta\right)$ can be seen as a constant value when implementing the levitation control. Therefore, the levitation forces can be controlled as that in magnetic bearings, which is easier and simpler compared with conventional BSRMs. In addition, as illustrated in Fig. 2, the output torque is provided in the torque region for each phase, thus the torque can be regulated as that in conventional SRMs, e.g. the CCC or APC method.

When CCC method is adopted to regulate output torque in the torque region of phase A, the required torque current i_T^* regulated by the closed-loop control of speed is tracked and conducted in the four coils of phase A. After that, when phase A is going into its levitation region, i_T^* is seen as the average current $\bar{i_a}$ in (6) and (7). Accordingly, Δi_{a1} and Δi_{a2} can be seen as the levitation currents i_α^* and i_β^*, which can be regulated by the closed-loop control of levitation in the two perpendicular directions, i.e. α and β axes. In fact, when the torque load increases, the reference current can be increased

accordingly till to the rated current of the phase winding. In that case, i_T^* can be the reference current of the winding which needs larger current. Δi_{a1} and Δi_{a2} can be used to calculate the other winding currents.Differently, when APC method is adopted, the turn-ON angle θ_{on} is then regulated by the closed-loop of speed. In this case, the current value at the point of transition from the torque region to the levitation region can be used as the average current $\bar{i_a}$. Accordingly, the levitation control is the same as that in CCC method.

B. Control Block

Fig. 11 shows the system control block of the proposed BSRM. The speed error is regulated by a PI controller to output the demanded torque current i_T^* in the CCC method or the demanded turn-ON angle θ_{on}^* in the APC method. The torque current or the turn-ON angle are used to regulate the winding currents in the torque region of each phase, as shown in Fig. 10. The two perpendicular radial displacements in the direction of α and β axes are detected through radial displacement sensors, respectively. The displacement errors are regulated by two PID controllers to output the levitation currents i_α^* and i_β^* in the levitation region of each phase, as shown in Fig. 10. The block of three-phase current distribution is to determine which phases and coils need to be conducted according to the rotor angle position θ. Finally, the switching signals are sent to the power converter to generate required winding currents.

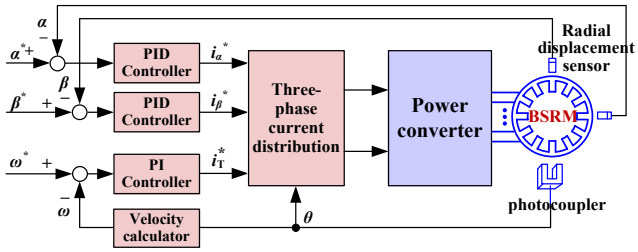

Fig. 11. System control block of proposed BSRM

IV. Experimental Results

In order to verify the demonstrated performance of proposed 12/4 BSRMs, the prototype with motor parameters listed in Table I is manufactured and the test rig is established to implement the proposed control methods. Figs. 12 and 13 shows the manufactured prototype and test rig. The asymmetric half-bridge circuit is adopted to excite the windings, and the TI TMS320F28335-based controller is used to implement the proposed control strategies and current algorithms. In experiments, the prototype is placed horizontally, except the radial-loading experiment. Two mechanical bearings are installed on the levitation end of the shaft, where one of them is the backup bearing to support and protect the shaft when the motor does not rotate or is not levitated as shown in Fig. 13(a), and the average clearance between the shaft and the inner ring of backup bearing is 200 μm. The other mechanical bearing is used to exert the radial load on the prototype as shown in Fig. 13(d), where the radial load is a 2-kg counterpoise and it exerts a 20 N pulling forces on the shaft through the loading ring. This mechanical bearing is installed between the shaft and the loading ring, and the counterpoise is drawn by a string fixed on the ring slot of the loading ring. In addition, the levitated end is connected to an eddy-current dynamometer via a bellow coupling when testing the torque loading performance as shown in Fig. 13(c). The non-levitated end of the shaft is supported by a ball bearing with tight fit. There is no torque transducer connected and the dynamometer is just used as a torque load. In the torque-loading experiments, based on the derived torque model and FEA method, the generated torque by the prototype was calculated approximately using the real winding currents. Finally, 0.2N·m was considered as the exerted torque load.

The radial displacements of the levitated end of the shaft are detected by eddy-current transducers, and the rotor angle position is measured by photocouplers at the non-levitated end of the shaft as shown in Fig. 13(b). The measured signals from eddy-current transducers, photocouplers, currents sensors are sent to the digital controller, and then the control algorithm illustrated in Fig. 11 is programmed and implemented by TI TMS320F28335. It is worth noting that the reference values of the torque and levitation currents are only obtained by the PI controller and the PID controller, respectively, which has greatly simplified the control of BSRMs. Compared with conventional 12/8 BSRMs, the complex current calculation is avoided, and the large look-up table is no longer needed to pre-store coefficients of torque and levitation-force models in the proposed 12/4 BSRMs. Finally, the reference torque and levitation currents are tracked by the power converter with twelve asymmetric half-bridge legs, as shown in Fig. 14.

A. Steady-State Performance

In order to verify the steady-state performance of the studied prototype, no-load experiments were completed at the speeds of 4000 r/min and 10000 r/min, respectively. Figs. 15, 16 and 17 show the experimental results. At the speed of 4000 r/min, the perpendicular radial displacements at the directions of α and β axes are both controlled within 50μm, which is much less than the clearance between the shaft and the inner ring of backup bearing. At the speed of 10000 r/min, the two radial displacements become larger but are still less than 80 μm. Therefore, the levitated end of shaft can be levitated steadily when the prototype is rotating at a high speed.

In the levitation control of BSRMs, the displacements of shaft are regulated indirectly by controlling the winding currents of bearingless motors, which has been shown in the control block as shown in Fig. 11. There are several factors that can lead to displacement oscillation, e.g. the commutation of three phases, the PID controller, the current control of power converters, the signal detection and A/D conversion of DSP, etc. In addition, the current stiffness and displacement stiffness which are determined by the parameters of studied prototype, could also cause the oscillation.

Fig. 18 shows the experimental results with 0.2N·m torque load at the speed of 8000 r/min. It can be seen that the radial displacement is less than 60 μm and the shaft is levitated steadily when the torque load is added.

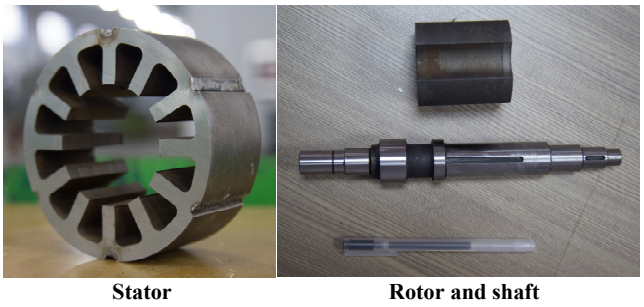

Fig. 12. Pictures of the test rig: (a) Stator, rotor and shaft. (b) Overview.

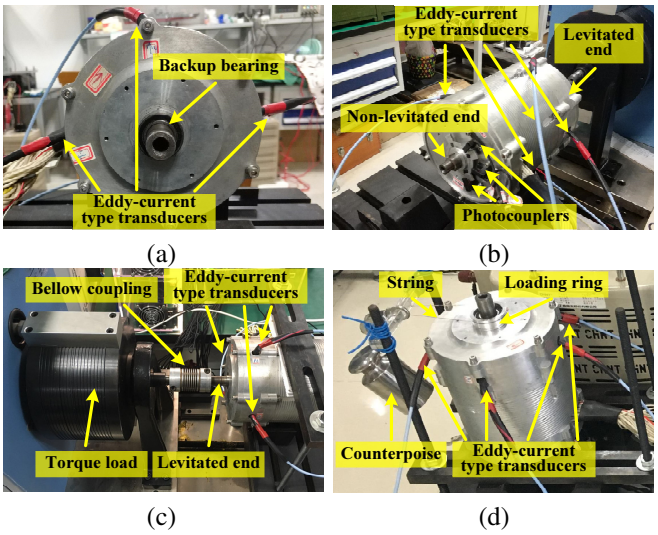

Fig. 13. Details of the prototype: (a) Backup bearing of the levitated end. (b) Photocouplers to detect rotor angle position and eddy-current type transducers to detect radial displacements. (c) Torque load. (d) Radial load.

B. Dynamic Performance in the Speed Changing Process

In order to test the dynamic performance of proposed methods, the motor speed was firstly increased from 6500 r/min to 7000 r/min and then decreased to 6500 r/min. Fig. 19 shows the experimental results. In this speed changing process, the two radial displacements almost keep the same as that in the steady state. Therefore, the levitation is not affected by the speed regulation.

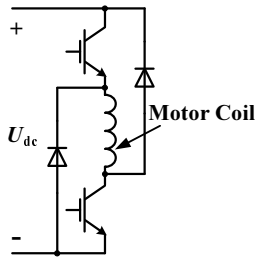

Fig. 14. Schematic view of one asymmetric half-bridge leg.

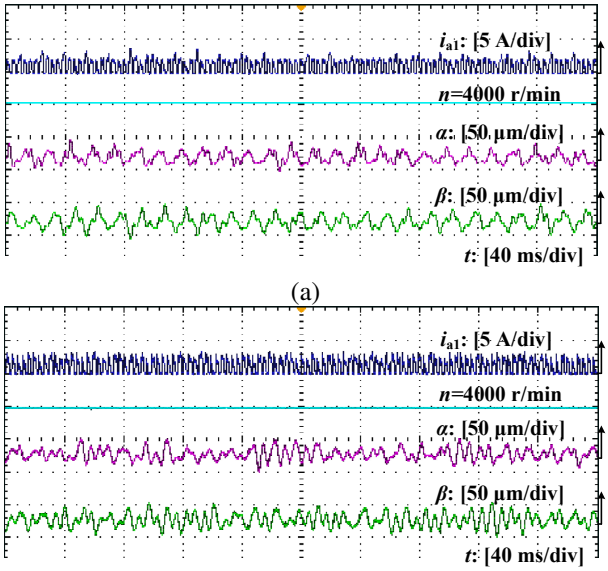

Fig. 15. Experimental results of shaft displacements at the speed of 4000 r/min with different control methods: (a) CCC method. (b) APC method.

C. Dynamic Performance in the Radial-Load Changing Process

In order to test the radial-load capability of proposed methods, a 2-kg counterpoise was firstly exerted to the shaft at the direction of α axis and then removed, as shown in Fig. 13(d). Fig. 20 shows the experimental results. With the two different control methods, the α-axis radial displacement firstly fluctuates by about 15 μm and then quickly back to the balanced position when the 20N radial load is added. When the radial load is removed, the α-axis radial displacement also firstly fluctuates about 15 μm and is then pulled back quickly to the balanced position. Moreover, the β-axis displacement is not affected by the radial-load variation at the direction of α-axis. Therefore, the two control methods have good dynamic performance on the radial-load variation.

D. Dynamic Performance with Sudden Knock on the Shaft

In addition, the experiments of sudden knock on the shaft were also completed to test the demonstrated performance. The shaft was knocked at the direction of α and β axes, respectively. Figs. 21 and 22 show the experimental results. It

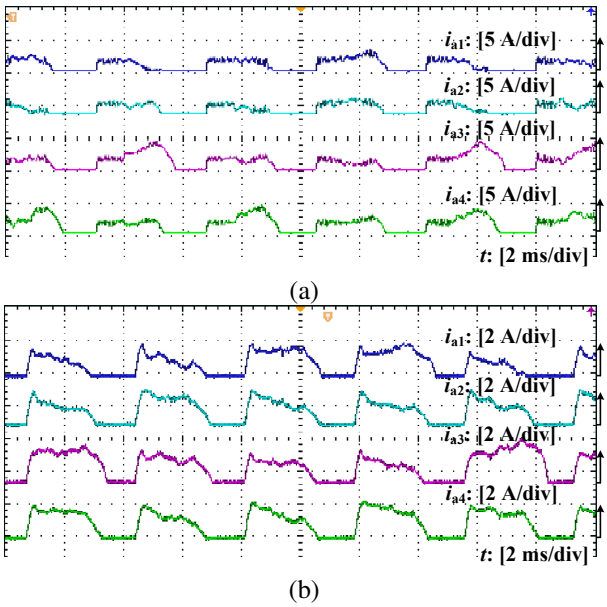

Fig. 16. Experimental waveforms of phase-A currents at the speed of 4000 r/min with different control methods: (a) CCC method. (b) APC method.

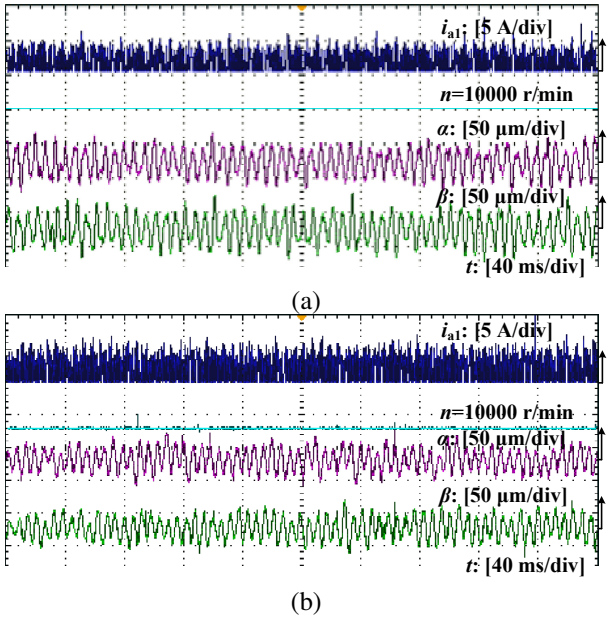

Fig. 17. Experimental results at the speed of 10000 r/min with different control methods: (a) CCC method. (b) APC method.

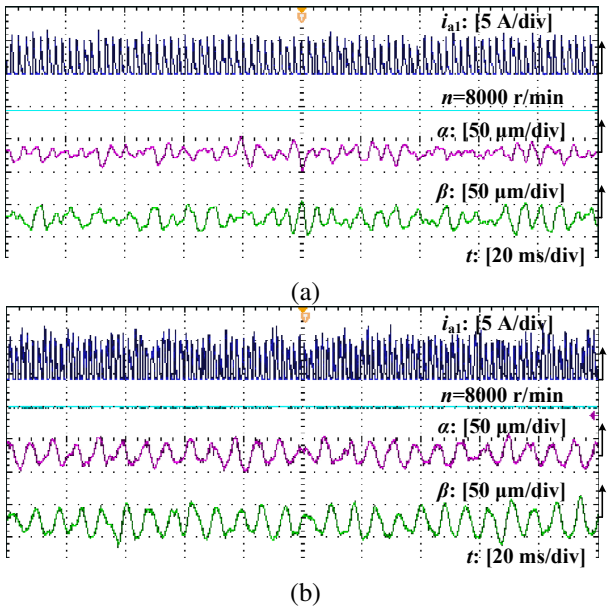

Fig. 18. Experimental results at the speed of 8000 r/min with 0.2N·m torque load. (a) CCC method. (b) APC method.

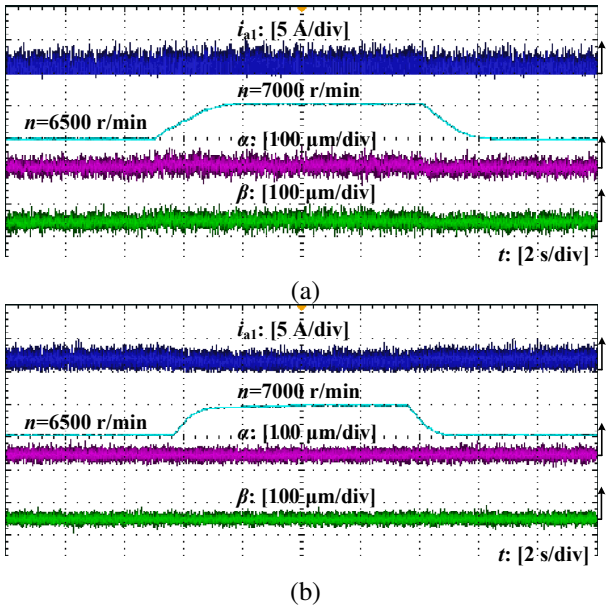

Fig. 19. Experimental results when the speed changes with different control methods: (a) CCC method. (b) APC method.

is noted that the radial displacement becomes large suddenly in the knock region. However, it can be pulled back in a very short time. Moreover, the radial displacement in the other direction is not affected by the sudden knock. Therefore, the proposed methods can also obtain a good performance when the sudden knock is exerted on the shaft.

E. Test on the Instability of Levitation Control

In order to test the performance on sudden removal of the levitation control, the PID parameters were changed to destabilize the levitation control. Fig. 23 shows the levitation waveforms from the stable levitation to shaft vibration and then to stillness. The shaft displacements can be limited within 50 μm with stable levitation, and the shaft rotates and vibrates greatly to its maximum limitation, i.e. 400 μm, because the average air-gap length between shaft and backup bearing is 200 μm. After that, the hardware circuits are protected to be OFF, and then the shaft becomes stillness to be supported by the backup bearing. When the shaft vibrates greatly, the inner ring of the backup bearing rotates with the shaft.

V. Conclusions

In this paper, the 12/4 BSRM is proposed to simplify the control of torque and levitation forces . By producing the

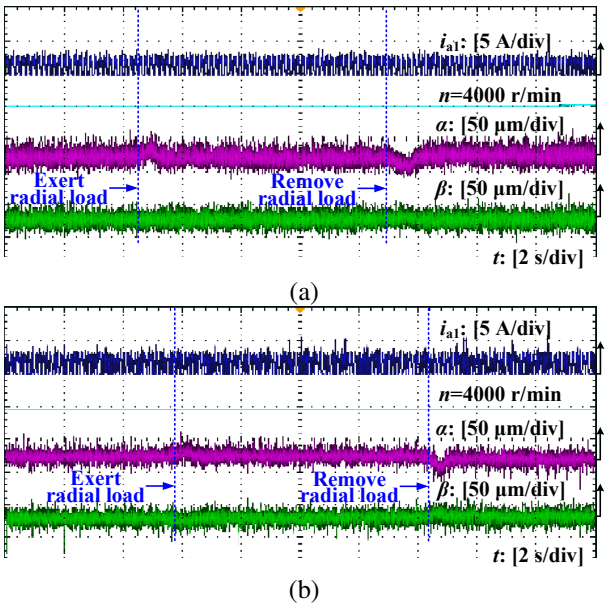

Fig. 20. Experimental results when the radial load changes with different control methods: (a) CCC method. (b) APC method.

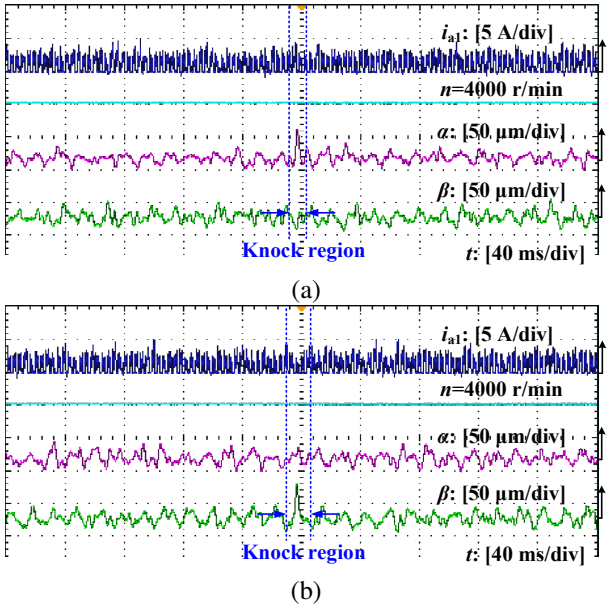

Fig. 21. Experimental results when knocking the shaft with CCC method: (a) α axis. (b) β axis.

torque and levitation forces in different regions of each phase, the coupling control of rotation and levitation is avoided, and the complex current algorithm is not needed neither. The levitation region is located in the flat region of maximum inductance, thus the levitation forces can be produced largely. Moreover, the levitation force can be regulated as that in the magnetic bearing, which greatly simplify the levitation control of BSRMs. In addition, the conventional torque control method for SRMs can also be used in the proposed BSRMs, which makes the rotation control more flexible. It is worth noting that the flat region of maximum inductance decreases the width of inductance-ascending region, hence the generation of the

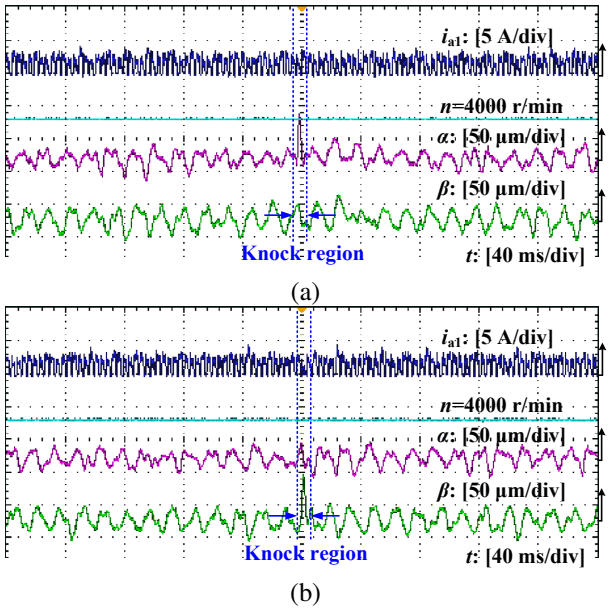

Fig. 22. Experimental results when knocking the shaft with APC method: (a) α axis. (b) β axis.

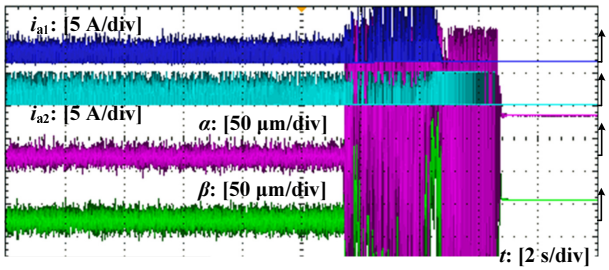

Fig. 23. Experimental results with the removal of levitation control.

positive torque is reduced. Therefore, it is a tradeoff between the rotation and the levitation in the design of BSRMs. Since the generation of levitation forces is like that in conventional magnetic bearings, the proposed BSRM is more suitable for the large radial-load application.

REFERENCES

[1] X. Deng, B. Mecrow, H. Wu, R. Martin, and Y. Gai, "Cost-effective and high-efficiency variable-speed switched reluctance drives with ring-connected winding configuration," *IEEE Trans. Energy Convers.*, vol. 34, no. 1, pp. 120–129, Mar. 2019.

[2] M. Mohamadi, A. Rashidi, S. M. S. Nejad, and M. Ebrahimi, "A switched reluctance motor drive based on quasi Z-source converter with voltage regulation and power factor correction," *IEEE Trans. Ind. Electron.*, vol. 65, no. 10, pp. 8330–8339, Oct. 2018.

[3] S. Song, G. Fang, Z. Zhang, R. Ma, and W. Liu, "Unsaturated-inductance-based instantaneous torque online estimation of switched reluctance machine with locally linearized energy conversion loop," *IEEE Trans. Ind. Electron.*, vol. 65, no. 8, pp. 6109–6119, Aug. 2018.

[4] X. Deng, B. Mecrow, H. Wu, and R. Martin, "Design and development of low torque ripple variable-speed drive system with six-phase switched reluctance motors," *IEEE Trans. Energy Convers.*, vol. 33, no. 1, pp. 420–429, Mar. 2018.

[5] A. Chiba, T. Fukao, O. Ichikawa, M. Oshima, M. Takemoto, and D. Dorrell, *Magnetic Bearings and Bearingless Drives*. Elsevier Science, 2005.

[6] M. Takemoto, K. Shimada, A. Chiba, and T. Fukao, "A design and characteristics of switched reluctance type bearingless motors," in *Proc. Int. Sym. Magn. Suspension Technol.*, vol. NASA/CP-1998-207654, 1998, pp. 49–63.

[7] M. Takemoto, H. Suzuki, A. Chiba, T. Fukao, and M. A. Rahman, "Improved analysis of a bearingless switched reluctance motor," *IEEE Trans. Ind. Appl.*, vol. 37, no. 1, pp. 26–34, Jan./Feb. 2001.

[8] M. Takemoto, A. Chiba, and T. Fukao, "A method of determining the advanced angle of square-wave currents in a bearingless switched reluctance motor," *IEEE Trans. Ind. Appl.*, vol. 37, no. 6, pp. 1702–1709, Nov./Dec. 2001.

[9] M. Takemoto, A. Chiba, H. Akagi, and T. Fukao, "Radial force and torque of a bearingless switched reluctance motor operating in a region of magnetic saturation," *IEEE Trans. Ind. Appl.*, vol. 40, no. 1, pp. 103–112, Jan./Feb. 2004.

[10] W.-T. Liu and S.-M. Yang, "Modeling and control of a self-bearing switched reluctance motor," in *Industry Applications Conference, 2005. Fourtieth IAS Annual Meeting. Conference Record of the 2005*, vol. 4, Oct. 2005, pp. 2720–2725.

[11] F.-C. Lin and S.-M. Yang, "Self-bearing control of a switched reluctance motor using sinusoidal currents," *IEEE Trans. Power Electron.*, vol. 22, no. 6, pp. 2518–2526, Nov. 2007.

[12] F.-C. Lin and S.-M. Yang, "An approach to producing controlled radial force in a switched reluctance motor," *IEEE Trans. Ind. Electron.*, vol. 54, no. 4, pp. 2137–2146, Aug. 2007.

[13] B. B. Choi and M. Siebert, "A bearingless switched reluctance motor for high specific power application," in *AIAA/ASME/SAE/ASEE Joint Propulsion Conf. Exhib.*, Sacramento, CA, Jul. 2006.

[14] L. Chen and W. Hofmann, "Speed regulation technique of one bearingless 8/6 switched reluctance motor with simpler single winding structure," *IEEE Trans. Ind. Electron.*, vol. 59, no. 6, pp. 2592–2600, Jun. 2012.

[15] C. R. Morrison, M. W. Siebert, and E. J. Ho, "Electromagnetic forces in a hybrid magnetic-bearing switched-reluctance motor," *IEEE Trans. Magn.*, vol. 44, no. 12, pp. 4626–4638, Dec. 2008.

[16] X. Cao, Z. Deng, G. Yang, and X. Wang, "Independent control of average torque and radial force in bearingless switched-reluctance motors with hybrid excitations," *IEEE Trans. Power Electron.*, vol. 24, no. 5, pp. 1376–1385, May 2009.

[17] J. Sun, Q. Zhan, and L. Liu, "Modelling and control of bearingless switched reluctance motor based on artificial neural network," in *Proc. 31st Annual Conf. of IEEE Industrial Electronics Society IECON 2005*, Nov. 2005.

[18] X. Cao, J. Zhou, C. Liu, and Z. Deng, "Advanced control method for a single-winding bearingless switched reluctance motor to reduce torque ripple and radial displacement," *IEEE Trans. Energy Convers.*, vol. 32, no. 4, pp. 1533–1543, Dec. 2017.

[19] Z. Zhu, Q. Wan, and Y. Sun, "An ELM identifier and inverse controller based algorithm for dynamic decoupling control of bearingless switched reluctance motor," in *2017 20th International Conference on Electrical Machines and Systems (ICEMS)*, Sydney, NSW, Australia, Aug. 2017, pp. 1–6.

[20] K. Yang, Z. Zhu, and Y. Sun, "Decoupling control of single winding bearingless switched reluctance motors based on support vector machine inverse system," in *2014 17th International Conference on Electrical Machines and Systems (ICEMS)*, Hangzhou, China, Oct. 2014, pp. 1829–1833.

[21] D.-H. Lee, H. Wang, and J.-W. Ahn, "Modeling and control of novel bearingless switched reluctance motor," in *Proc. IEEE Energy Conversion Congress and Exposition ECCE 2009*, Sept. 2009, pp. 276–281.

[22] H. Wang, Y. Wang, X. Liu, and J. W. Ahn, "Design of novel bearingless switched reluctance motor," *IET Proc. Electric Power Appli.*, vol. 6, no. 2, pp. 73–81, Feb. 2012.

[23] H. Wang, B. Xue, and S. Tang, "New type 12/14 bearingless switched reluctance motor with double windings," *IET Electr. Power Appl.*, vol. 9, no. 7, pp. 478–485, Jul. 2015.

[24] Z. Xu, D. H. Lee, and J. W. Ahn, "Comparative analysis of bearingless switched reluctance motors with decoupled suspending force control," *IEEE Trans. Ind. Appl.*, vol. 51, no. 1, pp. 733–743, Jan. 2015.

[25] X. Cao, H. Yang, L. Zhang, and Z. Deng, "Compensation strategy of levitation forces for single-winding bearingless switched reluctance motor with one winding total short circuited," *IEEE Trans. Ind. Electron.*, vol. 63, no. 9, pp. 5534–5546, Sep. 2016.

Zhenyang Hao received the B.Eng. degree from Nanjing Normal University, and the Ph.D. degree from Nanjing University of Aeronautics and Astronautics, Nanjing, China, in 2004 and 2010, respectively, both in Electrical Engineering.

Since 2010, he has been with Nanjing University of Aeronautics and Astronautics, where he is currently an Associate Professor at the Dept. of Electrical Engineering. From September 2014 to September 2015, he was a Visiting Scholar in Wisconsin Electric Machines and Power Electronics Consortium (WEMPEC), University of Wisconsin-Madison, U.S. His current research focuses on distributed generation and renewable energy, PMSM servo systems, and high speed machines.

Xin Cao (M'12) received the B.Eng., M.Sc., and Ph.D. degrees in electrical engineering from Nanjing University of Aeronautics and Astronautics, Nanjing, China, in 2003, 2006 and 2010, respectively.

Since 2011, he has been with Nanjing University of Aeronautics and Astronautics, where he is currently a Professor at the Dept. of Electrical Engineering. From June 2011 to September 2012, he was a Research Associate with the Department of Aeronautical and Automotive Engineering, Loughborough University, U.K. His current research focuses on distributed generation and renewable energy, switched reluctance machines, and high speed machines.

Xu Deng received the B.Eng. and M.Eng. degrees in Electrical Engineering from Nanjing University of Aeronautics and Astronautics, Nanjing, China, in 2010 and 2013, respectively. She received the PhD degree in Electrical Engineering from Newcastle University, Newcastle upon Tyne, U.K., in 2017.

She is currently a Research Associate of Electrical Power Research Group in the School of Engineering, Newcastle University, Newcastle upon Tyne, U.K. Her main researches are integrated drives and advanced control methods for power electronics and electric machines.

Xiang Shen received the Ph.D. degree in Mechanical Engineering from Queen Mary University of London, U.K., in 2017. He joined Newcastle University in the U.K. since 2018 to conduct multidisciplinary researches in mechanical design and thermal management on electric machines. In 2020, he became a Lecturer in Mechanical Engineering at Northumbria University, U.K., with research interests in mechanical design, thermal management, applied aerodynamics, wind engineering, aeroacoustics and multidisciplinary optimisation.